Int. J. Heat Mass Transfer. Vol. 14, pp. 1659–1675. Pergamon Press 1971. Printed in Great Britain

BOUNDARY VORTICITY METHOD FOR LAMINAR FORCED CONVECTION HEAT TRANSFER IN CURVED PIPES

MITSUNOBU AKIYAMA and K. C. CHENG

Department of Mechanical Engineering, University of Alberta, Edmonton, Alberta, Canada

(*Received* 17 *November* 1970 *and in revised form* 9 *February* 1971)

Abstract—A finite-difference solution using a combination of line iterative method and boundary vorticity method is presented for the hydrodynamically and thermally fully developed laminar forced convection in curved pipes subjected to the thermal boundary conditions of axially uniform wall heat flux and peripherally uniform wall temperature at any axial position. The numerical solution converges up to a reasonably high Dean number where the asymptotic behavior for the flow and heat transfer results already appears. The Prandtl number effect on heat transfer result is clarified for the first time, and it is shown that all the heat transfer results for $Pr \geqslant 1{\cdot}0$ can be correlated by a single curve using a new parameter (K^2Pr) with reasonable accuracy. The numerical results from the present analysis are compared with the experimental and theoretical results available in the literature. The perturbation method is clearly shown to be invalid, and certain deficiency of the boundary-layer approximation method is pointed out.

NOMENCLATURE

a, radius of pipe;
C, constant, $-C_1a^3/4\nu\mu$;
C_1, axial pressure gradient, $\partial P_0/Ra\partial\Omega$;
f, friction factor $2\bar{\tau}_w/(\rho\overline{W}^2)$ or a dummy variable;
$\bar{h}$ average heat transfer coefficient;
K, Dean number, $Re(a/R_c)^{\frac{1}{2}}$, see equation (19);
K_d, modified Dean number, $2^{\frac{1}{2}}K$, see equation (19);
k, thermal conductivity;
M, number of divisions in R-direction;
N, number of divisions in ϕ-direction;
Nu, Nusselt number, $\bar{h}(2a)/k$;
P, pressure;
P_0, axial pressure distribution measured along the centerline and a function of $R_c\Omega$ only;
P', pressure deviation which is a function of R and ϕ only;
Pr, Prandtl number, ν/α;
Q, a new parameter, $(K^2Pr)^{\frac{1}{2}}$;
$R, \phi, R_c\Omega$, cylindrical coordinates;
R_c, radius of curvature of a curved pipe;
Re, Reynolds number, $(2a)\overline{W}/\nu$;
r, dimensionless radial coordinate, R/a;
r_c, dimensionless radius of curvature of a curved pipe, R_c/a;
T, local temperature;
T_w, wall temperature;
U, V, W, velocity components in R, ϕ and $R_c\Omega$ directions;
u, v, w, dimensionless velocity components in r, ϕ and $r_c\Omega$ directions.

Greek letters

α, thermal diffusivity;
β, γ, σ, quantities defined in equation (13);
ε, a prescribed error, see equation (17);
θ, dimensionless temperature difference;
μ, viscosity;

ν, kinematic viscosity;
ζ, vorticity function defined by equation (9);
ρ, density;
τ, axial temperature gradient, $\partial T/R_c\partial\Omega$;
$\bar{\tau}_w$, mean shear stress at wall;
ψ, dimensionless stream function defined by equation (7);
ω, relaxation factor;
∇^2, dimensionless Laplacian operator.

Subscripts

b, value at boundary;
i, j, space subscripts of grid point in R and ϕ directions;
0, value for straight pipe;
w, value at wall.

Superscripts

n, nth iteration;
$^-$, average value.

1. INTRODUCTION

CURVED pipes or pipe bends are used extensively in industrial equipment such as helical coil or spiral heat exchangers, trombone coolers, reactors and various heat engines. The flow in curved pipes is characterized by Dean number with the double helix secondary flow acting in a cross-section normal to the main flow caused by centrifugal forces. Similar secondary flow patterns can also be caused by buoyancy forces in gravitational or rotating field, Coriolis forces and other body forces.

The literature on fully developed laminar flow in curved pipe is very extensive; but it appears that theoretical solution for hydrodynamic entrance flow in a curved pipe is not available. Similarly, the laminar forced convection heat transfer in curved pipes has been studied so far mainly for hydrodynamically and thermally fully developed regime only. Notably, one finds that the Graetz problem for curved pipes has not been solved yet. Under certain conditions, the effects due to buoyancy, Coriolis forces and angle of inclination must be considered simultaneously with the centrifugal force effect for the forced convection heat transfer in curved pipes. In contrast to the rather extensive data available for flow and heat transfer in straight pipes, it is evident that in many respects the corresponding design data for curved pipes are still lacking.

Focussing one's attention to the methods of analytical solution for fully developed laminar forced convection in curved pipes, it is found that the perturbation method [1, 2] is applicable only for very low Dean number flow regime. On the other hand, the approximate method [3–5] based on boundary layer concept near the pipe wall is valid only for high Dean number flow regime. For the intermediate Dean number flow regime, neither the perturbation method nor the boundary layer technique is effective.

The purpose of this paper is to present an accurate numerical solution using boundary vorticity method [6, 7] for a steady fully developed laminar forced convection in uniformly heated curved pipes valid up to a reasonably high value of the Dean number. This work was carried out as a first step toward the numerical solution of Graetz problem for curved pipes. In addition to presenting accurate flow and heat transfer results, the Prandtl number effect on laminar forced convection heat transfer in curved pipes is clarified for the first time. The numerical results for flow and heat transfer from this study will be compared with the data available in the literature, and the discrepancy will be clearly pointed out.

2. FORMULATION OF THE PROBLEM

Consideration is given to a steady hydrodynamically and thermally fully developed laminar flow of viscous incompressible fluid in a curved pipe under the thermal boundary conditions of axially uniform wall heat flux and peripherally uniform wall temperature at

any axial position. In order to facilitate the analysis, the following assumptions are made:

1. The radius of curvature of the pipe axis is large in comparison to the radius of the pipe.
2. Physical properties are constant and buoyancy effect is neglected.
3. Viscous dissipation is negligible and heat sources do not exist.

Taking the origin of the cylindrical coordinates $(R, \phi, R_c\Omega)$ at the center of the circular cross-section as shown in Fig. 1 and applying the assumptions stated above, the governing equations for the present problem can be shown to be [1]:

Continuity equation

$$\frac{\partial}{\partial R}(RU) + \frac{\partial V}{\partial \phi} = 0. \tag{1}$$

Momentum equations in R, ϕ and $R_c\Omega$ directions

$$U\frac{\partial U}{\partial R} + \frac{V}{R}\frac{\partial U}{\partial \phi} - \frac{V^2}{R} = -\frac{1}{\rho}\frac{\partial P'}{\partial R} - \frac{\nu}{R}\frac{\partial}{\partial \phi} \times \left(\frac{\partial V}{\partial R} + \frac{V}{R} - \frac{1}{R}\frac{\partial U}{\partial \phi}\right) + \frac{W^2}{R_c}\cos\phi \tag{2}$$

$$U\frac{\partial V}{\partial R} + \frac{V}{R}\frac{\partial V}{\partial \phi} + \frac{UV}{R} = -\frac{1}{\rho R}\frac{\partial P'}{\partial \phi} + \nu\frac{\partial}{\partial R} \times \left(\frac{\partial V}{\partial R} + \frac{V}{R} - \frac{1}{R}\frac{\partial U}{\partial \phi}\right) - \frac{W^2}{R_c}\sin\phi \tag{3}$$

$$U\frac{\partial W}{\partial R} + \frac{V}{R}\frac{\partial W}{\partial \phi} = -\frac{1}{\rho R_c}\frac{\partial P_0}{\partial \Omega} + \nu\left[\left(\frac{\partial}{\partial R} + \frac{1}{R}\right)\frac{\partial W}{\partial R} + \frac{1}{R}\frac{\partial}{\partial \phi}\left(\frac{1}{R}\frac{\partial W}{\partial \phi}\right)\right] \tag{4}$$

where the pressure at any point consists of two parts and is expressed as,

$$P = P_0(R_c\Omega) + P'(R, \phi).$$

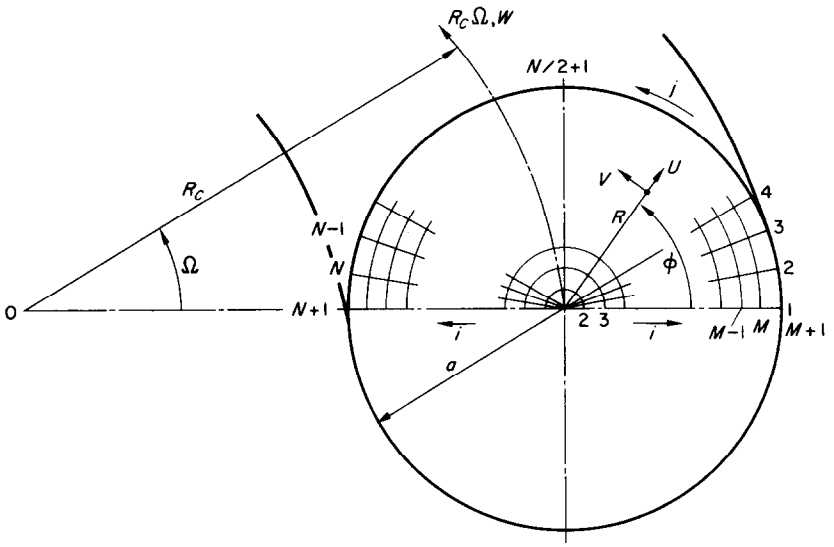

FIG. 1. Coordinate system and numerical grid.

Energy equation

$$U\frac{\partial T}{\partial R} + \frac{V}{R}\frac{\partial T}{\partial \phi} + \frac{W}{R_c}\frac{\partial T}{\partial \Omega} = \alpha\left(\frac{\partial^2 T}{\partial R^2} + \frac{1}{R^2}\frac{\partial^2 T}{\partial \phi^2} + \frac{1}{R}\frac{\partial T}{\partial R}\right). \tag{5}$$

The boundary conditions are:

$$U = V = W = T - T_w = 0 \qquad \text{at pipe wall.} \tag{6}$$

The simplified Navier–Stokes equations (2)–(4) and the energy equation (5) are quasi-linear, second-order partial differential equations of elliptic type. Introducing the following transformations,

$$R = [a]r, \qquad R_c = [a]r_c, \qquad U = [v/a]u,$$

$$V = [v/a]v, \qquad W = [Cv/a]w,$$
$$T_w - T = [C\tau Pr\, a]\theta, \qquad \partial P_0/R_c\partial\Omega = C_1,$$
$$-C_1a^3/4v\mu = C, \qquad \partial T/R_c\partial\Omega = \tau$$

and a dimensionless stream function ψ,

$$u = \frac{1}{r}\frac{\partial\psi}{\partial\phi}, \qquad v = -\frac{\partial\psi}{\partial r} \tag{7}$$

the momentum and energy equations can be restated in the following dimensionless forms after eliminating pressure terms between equations (2) and (3).

Momentum equation for secondary flow

$$u\frac{\partial\zeta}{\partial r} + \frac{v}{r}\frac{\partial\zeta}{\partial\phi}$$

$$= \nabla^2\zeta - 2\left(\frac{C^2}{r_c}\right)w\left(\frac{1}{r}\cos\phi\frac{\partial w}{\partial\phi} + \sin\phi\frac{\partial w}{\partial r}\right) \tag{8}$$

where

$$\nabla^2 = \frac{\partial^2}{\partial r^2} + \frac{1}{r}\frac{\partial}{\partial r} + \frac{1}{r^2}\frac{\partial^2}{\partial\phi^2}.$$

Vorticity equation

$$\zeta = \nabla^2\psi. \tag{9}$$

Axial momentum equation

$$u\frac{\partial w}{\partial r} + \frac{v}{r}\frac{\partial w}{\partial\phi} = \nabla^2 w + 4. \tag{10}$$

Energy equation

$$Pr\left(u\frac{\partial\theta}{\partial r} + \frac{v}{r}\frac{\partial\theta}{\partial\phi}\right) = \nabla^2\theta + w. \tag{11}$$

It is noted that the vorticity function ζ is introduced here to avoid using biharmonic function $\nabla^4\psi$ in the momentum equation for secondary flow. Because of symmetry it is only required to consider, for example, the upper half of the circular region (see Fig. 1). The boundary conditions are now restated as follows:

$$\psi = \frac{\partial\psi}{\partial r} = w = \theta = 0 \quad \text{at pipe wall } (r = 1)$$

$$\psi = \zeta = \frac{\partial w}{\partial\phi} = \frac{\partial\theta}{\partial\phi} = 0 \quad \begin{matrix}\text{along horizontal center}\\ \text{line } (\phi = 0 \text{ and } \pi).\end{matrix} \tag{12}$$

In contrast to the forced convection with secondary flow caused by buoyancy forces, a set of momentum equations (8)–(10) is seen to be uncoupled with the energy equation (11) and the flow problem can be solved independently. Since a perturbation method [1, 2] is known to diverge quickly with the increase of Dean number, a numerical solution appears to be the only practical approach for the accurate solution of the present problem. By substituting the vorticity function into the momentum equation (8) for secondary flow, the vorticity function can be eliminated, but the numerical solution of the resulting set of equations in cylindrical coordinates by the conventional method [8] is known to converge extremely slowly and is not practical from the viewpoint of computing time. Because of recent development of the boundary vorticity method [6], the above difficulty can be overcome readily.

3. FINITE DIFFERENCE APPROXIMATIONS AND BOUNDARY VORTICITY METHOD

By using a three-point central-difference approximation and a dummy variable f for the dependent variables w, ζ, ψ and θ, a general finite-difference equation can be written for equations (8)–(11) as follows:

$$\left[1 - \frac{\Delta r}{2r_i} + \beta\right] f_{i-1,j} + \left[-2 - 2\left(\frac{\Delta r}{r_i \Delta\phi}\right)^2\right] f_{i,j} + \left[1 + \frac{\Delta r}{2r_i} - \beta\right] f_{i+1,j}$$

$$= -\left[\left(\frac{\Delta r}{r_i \Delta\phi}\right)^2 + \gamma\right] f_{i,j-1} + \left[-\left(\frac{\Delta r}{r_i \Delta\phi}\right)^2 + \gamma\right] f_{i,j+1} + \sigma \qquad (13)$$

where,

$$\beta = \begin{cases} \frac{\Delta r}{2} u_{i,j} \\ 0 \\ \frac{\Delta r}{2} Pr\, u_{i,j} \end{cases}, \quad \gamma = \begin{cases} \frac{(\Delta r)^2}{2r_i \Delta\phi} v_{i,j} & \text{for } f_{i,j} = \zeta_{i,j} \text{ and } w_{i,j} \\ 0 & \text{for } f_{i,j} = \psi_{i,j} \\ \frac{(\Delta r)^2}{2r_i \Delta\phi} Pr\, v_{i,j} & \text{for } f_{i,j} = \theta_{i,j} \end{cases}$$

$$\sigma = \begin{cases} \left(\frac{C^2}{r_c}\right) w_{i,j} \left[\frac{(\Delta r)^2}{r_i \Delta\phi} (w_{i-1,j} - w_{i+1,j}) \cos\phi_j + (w_{i,j-1} - w_{i,j+1}) \sin\phi_j\right] & \\ & \text{for } f_{i,j} = \zeta_{i,j} \\ -(\Delta r)^2 \zeta_{i,j} & \text{for } f_{i,j} = \psi_{i,j} \\ -(\Delta r)^2\, 4 & \text{for } f_{i,j} = w_{i,j} \\ -(\Delta r)^2 w_{i,j} & \text{for } f_{i,j} = \theta_{i,j}. \end{cases}$$

In order to circumvent the singularity at the origin of the cylindrical coordinates, finite difference equation in Cartesian coordinates is employed at the origin instead of the usual approximate or extrapolation method.

For the purpose of illustrating the computational procedure using boundary vorticity method, a set of finite-difference equations for secondary flow obtained by applying equation (13) to the grid points along the radial line $j = l$ will be written in a matrix form as follows:

$$\begin{bmatrix} B_2 & C_2 & & & & & \\ A_3 & B_3 & C_3 & & 0 & & \\ & A_4 & B_4 & C_4 & & & \\ & & \cdot & \cdot & \cdot & & \\ & & & \cdot & \cdot & \cdot & \\ & 0 & & & A_{M-1} & B_{M-1} & C_{M-1} \\ & & & & & A_M & B_M \end{bmatrix} \begin{bmatrix} \zeta_{2,l} \\ \zeta_{3,l} \\ \zeta_{4,l} \\ \cdot \\ \cdot \\ \zeta_{M-1,l} \\ \zeta_{M,l} \end{bmatrix} = \begin{bmatrix} G_{2,l} \\ G_{3,l} \\ G_{4,l} \\ \cdot \\ \cdot \\ G_{M-1,l} \\ G_{M,l} - C_M \zeta_{M+1,l} \end{bmatrix} \qquad (14)$$

Here the symbols A_i, B_i and C_i represent the coefficient for the dependent variables $\zeta_{i-1,l}$, $\zeta_{i,l}$ and $\zeta_{i+1,l}$ respectively, in equation (13) at the grid point (i, l) and the symbol $G_{i,l}$ represents all the terms on the right hand side of the same equation for $f_{i,l} = \zeta_{i,l}$. Similarly, by considering the radial line $j = l$, a set of linear algebraic equations for the stream function $\psi_{i,l}$ can be written in a matrix form as

$$\begin{bmatrix} E_2 & F_2 & & & & & & \\ D_3 & E_3 & F_3 & & & 0 & & \\ & D_4 & E_4 & F_4 & F_4 & & & \\ & & \cdot & \cdot & \cdot & & & \\ & & & \cdot & \cdot & \cdot & & \\ & 0 & & & D_M & E_M & F_M & \\ & & & & & (D_{M+1} + F_{M+1}) & E_{M+1} \end{bmatrix} \begin{bmatrix} \psi_{2,l} \\ \psi_{3,l} \\ \psi_{4,l} \\ \cdot \\ \cdot \\ \psi_{M,l} \\ \psi_{M+1,l} \end{bmatrix} = \begin{bmatrix} H_{2,l} \\ H_{3,l} \\ H_{4,l} \\ \cdot \\ \cdot \\ H_{M,l} \\ H_{M+1,l} \end{bmatrix} \tag{15}$$

where D_i, E_i and F_i stand for the coefficient of the stream functions $\psi_{i-1,l}$, $\psi_{i,l}$ and $\psi_{i+1,l}$ respectively, in equation (13) at the grid point (i, l), and $H_{i,l}$ denotes all the terms on the right hand side of the same equation when $f_{i,l} = \psi_{i,l}$.

It is noted that equations (14) and (15) are obtained after applying the boundary conditions $\zeta_{i,1} = \zeta_{i,N+1} = \zeta_{1,j} = 0$ for equation (8), and the boundary conditions $\psi_{i,1} = \psi_{i,N+1} = \psi_{1,j} = 0$ and $\partial\psi_{M+1,j}/\partial r = 0$ (or $\psi_{M,j} = \psi_{M+2,j}$) for equation (9). The success of the boundary vorticity method is based on the observation that a linear relationship exists between the vorticity function $\zeta_{M+1,l}$ and the stream function $\psi_{M+1,l}$ at the boundary [6, 7]. For example, given three sets of values at a boundary point for the vorticity function and the stream function, namely, $\zeta_b^{(1)}$ and $\psi_b^{(1)}$, $\zeta_b^{(2)}$ and $\psi_b^{(2)}$, and $\zeta_b^{(3)}$ and $\psi_b^{(3)}$, the following linear relationship exists.

$$\zeta_b^{(3)} = \frac{\zeta_b^{(2)} - \zeta_b^{(1)}}{\psi_b^{(2)} - \psi_b^{(1)}}(\psi_b^{(3)} - \psi_b^{(2)}) + \zeta_b^{(2)}. \tag{16}$$

At the beginning one assumes that $\zeta_{M+1,l} = \zeta_b^{(1)}$ in equations (14) and (15). Then equation (14) can be solved simultaneously for $\zeta_{i,l}$, $i = 2, 3, \ldots M$, by using the Gaussian elimination method. Using the obtained vorticity functions, the right hand column of the matrix equation (15) can be evaluated. Applying the Gaussian elimination method to equation (15), the values for the stream function $\psi_{i,l}$ can be found, and the boundary value $\psi_{M+1,l} = \psi_b^{(1)}$ will be stored. By assuming again $\zeta_{M+1,l} = \zeta_b^{(2)}$ and following exactly the same procedure, the second boundary value $\psi_{M+1,l} = \psi_b^{(2)}$ will also be stored. Using the linear relation (16) and noting that $\psi_b^{(3)} = 0$, $\zeta_b^{(3)}$ can be obtained. Substituting the newly obtained boundary vorticity $\zeta_b^{(2)}$ into equations (14) and (15) and solving these equations, one obtains $\zeta_{i,l}$ and $\psi_{i,l}$, $i = 2, 3, \ldots M$, which represent the numerical solutions along the radial line $j = l$. The same computational procedure will be repeated for the succeeding radial lines $j = l + 1, l + 2, \ldots$ etc. with $j = 2$ at the beginning. Numerical experiments show that using $\zeta_b^{(3)}$ the values of the stream function on the boundary, $\psi_{M+1,l}$, range from 10^{-7} to 0 as compared with the largest value at interior point. Theoretically, of course, the stream function must vanish at the boundary. It is noted that an error of the above magnitude may be caused by a round-off error using a single precision.

With a computational procedure for the numerical determination of the boundary vorticity established, it suffices to mention that the usual line iterative relaxation method [6, 7] for the numerical solution of a set of finite-difference equations with the associated boundary conditions may be employed.

In the numerical computation, the prescribed error for all the dependent variables and the secondary velocity components is

$$\varepsilon = \sum_{i,j}^{\substack{M+1 \\ N+1}} \left| f_{i,j}^{(n+1)} - f_{i,j}^{(n)} \right| \Big/ \sum_{i,j}^{\substack{M+1 \\ N+1}} \left| f_{i,j}^{(n+1)} \right| < 10^{-5}. \tag{17}$$

Since the momentum equations (8) and (10) are coupled, the number of inner iterations involving the boundary vorticity method is of some interest. The following result is found to be satisfactory from the viewpoint of computing time after some numerical experiments:

Number of inner iterations relating to boundary vorticity method	$(f\,Re)/(f\,Re)_0$
20 ~ 50	1·0 ~ 1·1
20 ~ 5	1·1 ~ 1·35
1	1·35 or higher.

The parameter $f\,Re$ will be defined later. The number of inner iterations for $w_{i,j}$ is always one. It is noted that further increase of the number of inner iterations may destabilize the convergence of the iteration process.

In order to accelerate the convergence, an overrelaxation factor is used. Since nonlinear terms are involved in the elliptic type partial differential equations for the present problem, no general method is available for the evaluation of an optimum relaxation factor. However, with a mesh size of M, $N = 28$, a relaxation factor ranging from 1·7 for small Dean number to 1·0 for large Dean number is found to be satisfactory for all the equations except the momentum equation (8) for secondary flow where a factor of 1·0 is used always in the numerical computation. In order to stabilize the convergence in the high Dean number region, underrelaxation factors of 0·7, 0·5, 0·1 and 0·02 are also tried. However, no appreciable difference is observed in extending the parametric value as compared with the relaxation factor of 1·0, confirming that the boundary vorticity method is computationally very stable.

The convergence of the iteration process depends on whether or not the coefficient matrix is diagonally dominant. Consider, for example, an off-diagonal element

$$A_i = 1 - \frac{\Delta r}{2r_i} + \frac{\Delta r}{2} u_{i,l}$$

in equation (14). To ensure diagonal dominance, one expects a restriction on the magnitude of the secondary flow velocity component to be $|u_{i,l}| < (2/\Delta r - 1/r_i)$. If the limit is exceeded, the coefficient may no longer be diagonally dominant, and the numerical solution starts oscillation and finally diverges. This difficulty can be overcome by using finer mesh sizes, but the computing time and the round-off errors increase correspondingly. In order to extend the numerical solution into high parameter region, the mesh sizes of M, $N = 56$ and $M = 74$, $N = 42$ are also tried in some cases in addition to the mesh size of M, $N = 28$ for most computations.

At this point a comparison between the boundary vorticity method and the conventional methods of determining the boundary vorticity is of practical interest. One may determine the

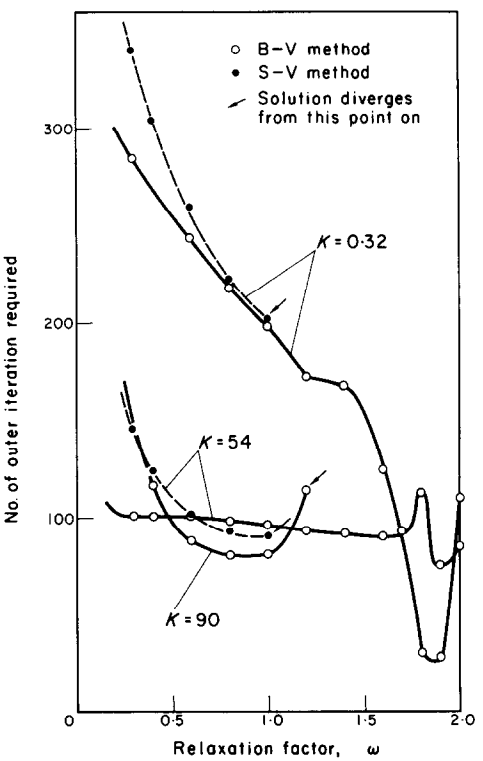

FIG. 2. Comparison of numerical solution between boundary vorticity method and stream function–vorticity method.

boundary vorticity by unsteady state method [9] or writing the central finite difference equation for equation (9) at the boundary leading to the following expression:

$$\zeta_{M+1,j} = 2\psi_{M,j}/(\Delta r)^2.$$

The approximation of the boundary vorticity is known to have a significant effect on the stability of numerical solution. Using the above expression for boundary vorticity, a set of the governing equations can be solved by the conventional line iterative method. This method of solution will be referred to as stream function-vorticity method in this paper. Figure 2 illustrates the results of numerical experiments for the boundary vorticity method and the stream function–vorticity method at the values of Dean number $K = 0{\cdot}32$, 54 and 90, respectively. For this comparison, the number of inner iterations is fixed. At $K = 0{\cdot}32$ and 54, the stream function–vorticity method fails to yield convergent solution with the restriction of equation (17) for relaxation factor $\omega \geqslant 1$. In particular, the stream function–vorticity method fails to yield convergent solution for $K = 90$ even with an underrelaxation factor as small as $\omega = 0{\cdot}05$. In contrast, the boundary vorticity method converges quickly with $\omega = 0{\cdot}8 \sim 1{\cdot}0$. In high Dean number range, the boundary vorticity method has definite advantage.

4. FLOW AND HEAT TRANSFER RESULTS

It is possible to obtain the expressions for the product of friction factor and Reynolds number ($f\,Re$) and Nusselt number (Nu) by considering either the velocity and temperature gradients, respectively, along the pipe wall, or the overall force and energy balances, respectively, for the axial length $R_c d\Omega$. The results are

$$\begin{aligned}(f\,Re)_{\mathrm{I}} &= 4\left|\overline{\partial w}/\partial r\right|_w/\overline{w}\\ (Nu)_{\mathrm{I}} &= 2\overline{w}\left|\overline{\partial\theta}/\partial r\right|_w/\left|\overline{w\theta}\right|\\ (f\,Re)_{\mathrm{II}} &= 8/\overline{w}\\ (Nu)_{\mathrm{II}} &= \overline{w}^2/\left|\overline{w\theta}\right|.\end{aligned} \tag{18}$$

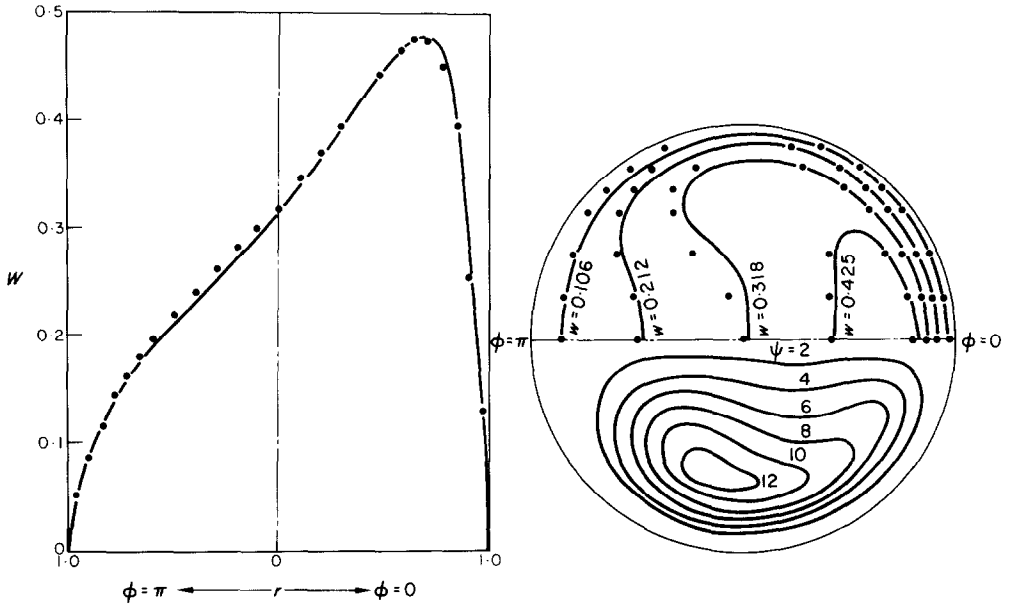

FIG. 3. Comparison of velocity profile along $\phi = 0$ and π and isolines for velocity at $K = 196$ from this work with Adler's experimental data at $K = 205$ and streamlines at $K = 196$ from this work.

Evaluation of the mean values indicated above are carried out by using Simpson's rule. The above two expressions for the overall characteristics, $f\,Re$ and Nu, afford checking the congence of the numerical results. It is of interest to note that the Dean number K and the modified Dean number K_d can be written as

$$K = 2\left(\frac{C^2}{r}\right)^{\frac{1}{4}} \bar{w} = Re\left(\frac{a}{R_c}\right)^{\frac{1}{2}}$$

$$K_d^2 = 2K^2 = ReRe_c = \left(\frac{\rho \overline{W}^2/2a}{\mu \overline{W}/(2a)^2}\right)\left(\frac{\rho \overline{W}^2/R_c}{\mu \overline{W}/(2a)^2}\right). \tag{19}$$

The parameter Re_c represents the ratio of the centrifugal force effect to the viscous force effect and might be referred to as centrifugal Reynolds number.

equation (17). The streamlines are also illustrated in Fig. 3, and one sees that at $K = 196$ the center of circulation is situated near the inner wall. The loci of the centers of circulation are of interest. As Dean number increases, the centers of circulation move toward the wall radially, but horizontally they move away first from the central vertical axis toward the outer wall. With further increase of Dean number they then move back toward the inner wall. The distribution of the secondary flow velocity is unsymmetric with respect to the central vertical axis. Furthermore, the distribution of the streamlines suggests that at $K = 196$, the boundary layer approximation cannot be applied.

The effect of Dean number on average friction factor is well understood. The effect of Dean

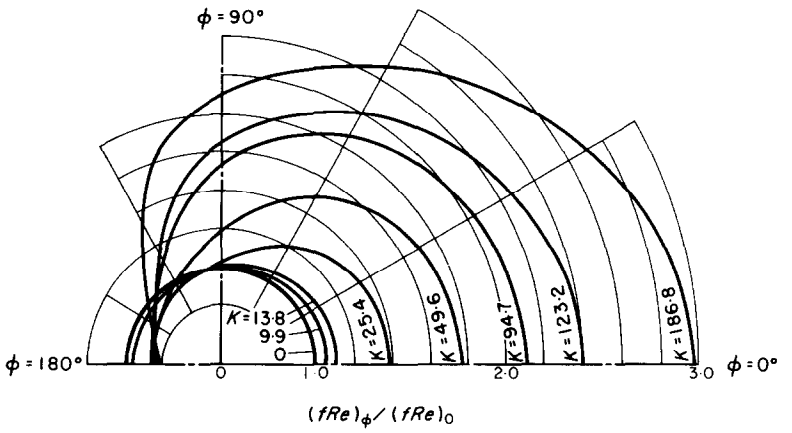

FIG. 4. Local angular distribution of $(f\,Re)_\phi/(f\,Re)_0$ with Dean number K as a parameter.

In order to assess the accuracy of the numerical solution, the axial velocity profile along the central horizontal axis and isolines for velocity from this analysis at $K = 196$ are compared against Adler's experimental data [3] at $K = 205$ in Fig. 3. A good agreement is observed between the present numerical solution and the experimental data. The numerical solution can be extended to $K = 205$ with relaxation of the prescribed error but the numerical results at $K = 196$ are based on

number on the local distribution of friction factor is of theoretical interest but appears to have not been reported in the literature. Figure 4 shows the local angular distribution of $(f\,Re)_\phi/(f\,Re)_0$ as K varies from 0 to 186·8. At $K = 13{\cdot}8$ the value of $(f\,Re)_\phi/(f\,Re)_0$ is seen to be larger than one along the outer wall $(-\pi/2 < \phi < \pi/2)$ and less than one along the inner wall such that the average value is slightly larger than one. At $K = 94{\cdot}7$, the region with $(f\,Re)_\phi > f\,Re)_0$ occupies nearly three-quarters of the whole

region including the outer wall. With further increase of Dean number, the value of $(fRe)_\phi/(fRe)_0$ is always seen to be less than one in the neighbourhood of $\phi = \pi$.

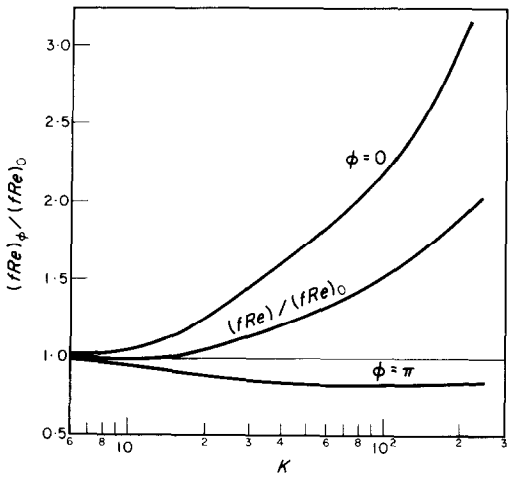

FIG. 5. $(fRe)_\phi/(fRe)_0$ vs. K at outer surface ($\phi = 0$) and inner surface ($\phi = \pi$) with comparison made against $fRe/(fRe)_0$.

In order to bring out the effect of Dean number on local friction factor more clearly, the value of $(fRe)_\phi/(fRe)_0$ is plotted against K in Fig. 5 for $\phi = 0$ and $\phi = \pi$, together with the average value $(fRe)/(fRe)_0$ indicated for comparison. In very low Dean number region, say up to $K = 10$, the centrifugal force effect on the average value of fRe is negligible, but one can clearly see the difference between the local value at $\phi = 0$ (or $\phi = \pi$) and the average value. Within the range of present investigation one notes that both the local value of $(fRe)_\phi$ at $\phi = 0$ and the average value increase continuously with K, but the local value of $(fRe)_\phi/(fRe)_0$ at $\phi = \pi$ remains at around 0·84 after reaching say $K = 40$.

Fully developed laminar flow in curved pipes has been studied very extensively in the past because of its technical importance. Figure 6 shows the comparison between the result of present numerical analysis and the experimental and theoretical data available in the literature

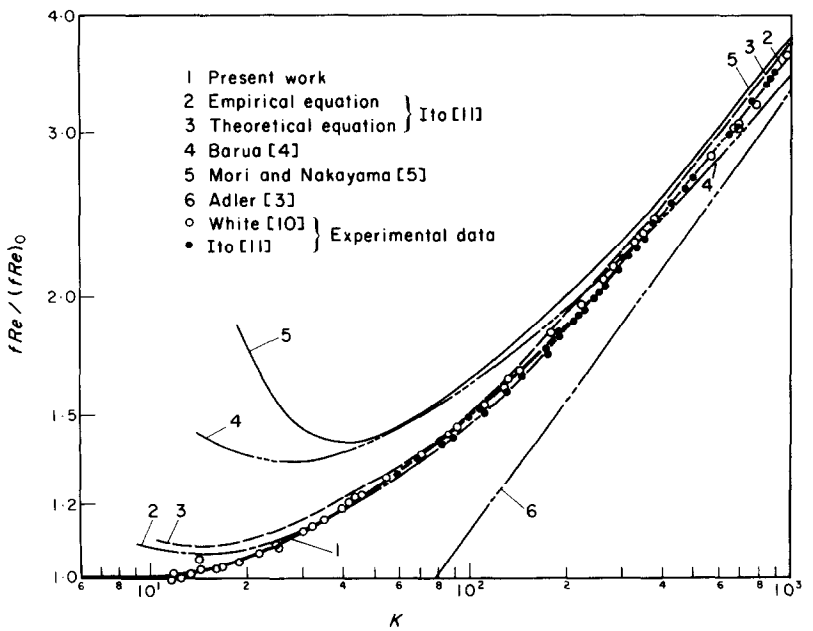

FIG. 6. Comparison of friction factor results from this work with theoretical and experimental results available in literature.

for $fRe/(fRe)_0$ vs. Dean number K. It is seen clearly that the present result agrees with the experimental data of White [10] and Ito [11] from relatively small to high Dean number region, while the predictions based on boundary layer approximation [3–5] lead to completely wrong trend in the low Dean number region. Ito's prediction is generally good for the range of Dean numbers under consideration, but has some error in the low parameter range. The above comparison serves to illustrate the relative merits of the various theoretical methods. For the high Dean number region, Ito's prediction deserves to be used in design.

expected that the secondary flow due to centrifugal force is rather weak. An examination of the energy equation (11) reveals that the role of Prandtl number in convective terms is similar to that of Dean number, and this observation is confirmed by the temperature profiles shown in Fig. 7. The temperature profile along the central vertical axis exhibits saddle shape in the central region, indicating a rather dominant convective motion therein. One should point out that the characteristics noted above for the temperature field are further magnified with the increase of the parameters K and Pr within the range of the present investigation. Unfortunately the present

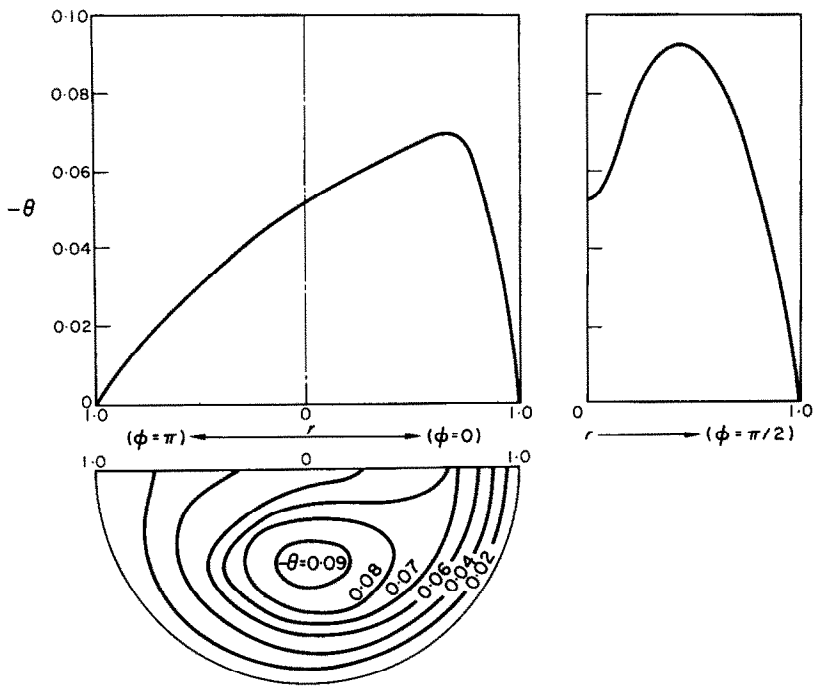

FIG. 7. Temperature profiles and isothermals at $K = 7{\cdot}66$ for $Pr = 100$.

Typical temperature profiles along the central horizontal and vertical axes and isothermals from the present analysis for $Pr = 100$ and $K = 7{\cdot}66$ are shown in Fig. 7. At $K = 7{\cdot}66$ it is

numerical solution cannot reach the value of $K = 632$ to enable one to make direct comparison with the experimental temperature profiles for air reported by Mori and Nakayama [5].

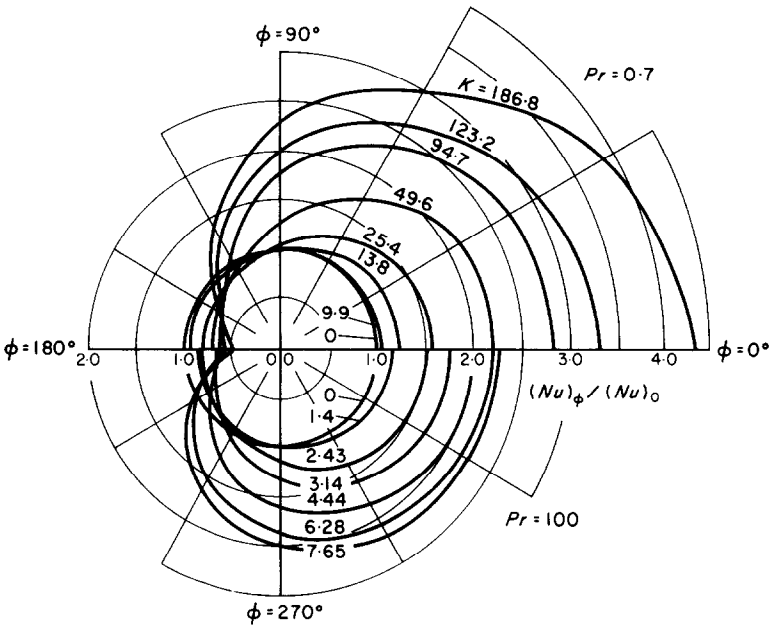

FIG. 8. Local angular distribution of $(Nu)_\phi/(Nu)_0$ with Dean number K as a parameter for $Pr = 0{\cdot}7$ and 100.

However, one notes a significant difference for temperature profile along central horizontal axis in the neighborhood of inner wall ($\phi = \pi$), with the present numerical result and the experimental data lying on opposite sides of the temperature profile for a straight pipe.

In order to consider the above discrepancy further, the angular distribution of the local Nusselt number along the pipe wall with Dean number as a parameter is shown in Fig. 8 for $Pr = 0{\cdot}7$ and 100. The variations of the local Nusselt numbers at $\phi = 0$ (outer wall) and $\phi = \pi$ (inner wall) with Dean number K, are shown in Fig. 9 for $Pr = 0{\cdot}7$, with the average Nusselt number included for comparison. As expected, the situation is similar to that shown in Fig. 5 for friction factor.

The overall heat transfer results in terms of the Nusselt number ratio $Nu/(Nu)_0$ vs. Dean number K from this analysis are shown in Fig. 10 for various Prandtl numbers with comparison made against Özisik and Topakoglu's results [2] using perturbation method, Mori and Nakayama's theoretical results using boundary layer

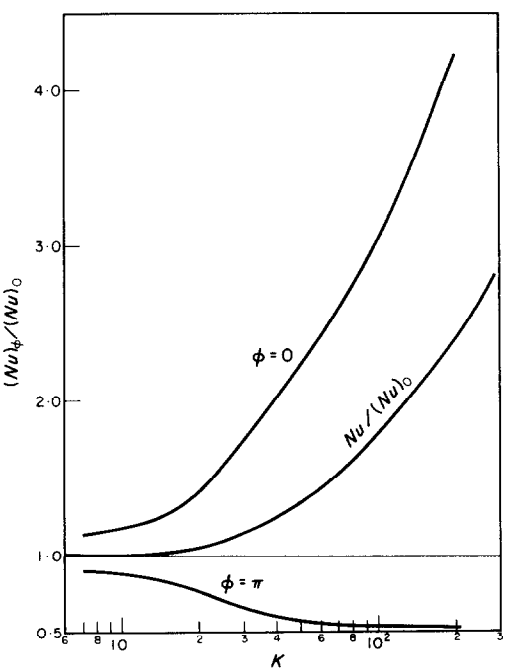

FIG. 9. $(Nu)_\phi/(Nu)_0$ vs. K at outer surface ($\phi = 0$) and inner surface ($\phi = \pi$) with comparison made against $Nu/(Nu)_0$ for $Pr = 0{\cdot}7$.

approximation and their experimental data [5], and also Seban and McLaughlin's experimental data [12]. It is noted that the data obtained by Seban and McLaughlin [12] are reproduced here by using the same transformation as that used by Özisik and Topakoglu [2]. It can be seen that the average Nusselt number from this analysis is closer to the experimental data at outer surface than those at inner surface given by Seban and McLaughlin [12]. For $Pr = 0{\cdot}7$ (air) the result from the layer approximation is valid near $Pr = 1{\cdot}0$ only, and the result for $Pr = \infty$ shown in [5] is believed to be invalid. The existence of asymptotic value for $Pr \to \infty$ is doubtful; but the asymptotic value does indeed exist for $Pr \to 0$, as shown in Fig. 10.

The effect of Prandtl number on forced convective heat transfer in curved pipes is of considerable theoretical and practical interest. A careful study of the heat transfer results for $Pr > 1$ shown in Fig. 10 reveals that after

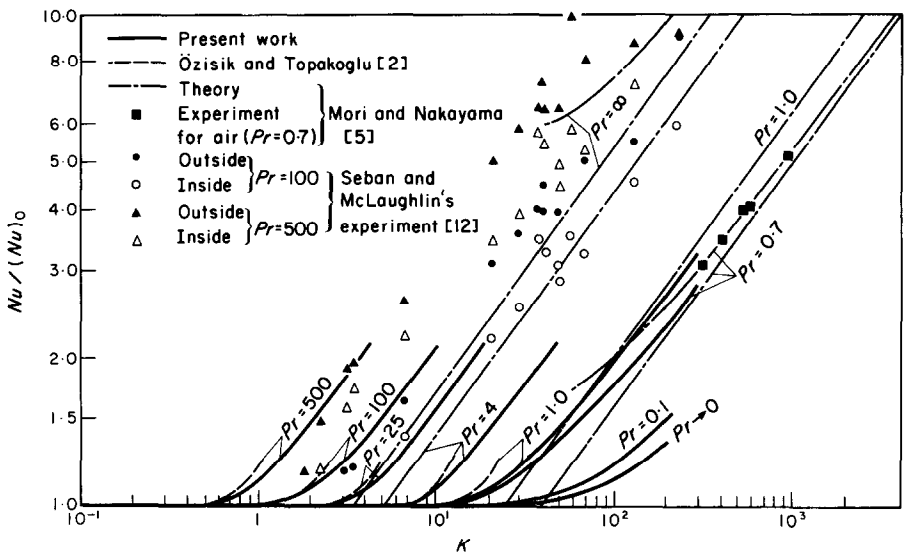

FIG. 10. Comparison of heat transfer results from this work with theoretical and experimental results available in literature.

present analysis agrees with Mori and Nakayama's data [5] for air. As can be clearly seen, Özisik and Topakoglu's results from perturbation method diverge quickly with the increase of Dean number. It is now evident that the perturbation method cannot be applied to the forced convective heat transfer with secondary flow except in a very low parameter region which is practically not important. Based on the results from this analysis, it appears that Mori and Nakayama's theoretical result from boundary reaching a certain Dean number or $Nu/(Nu)_0 \approx 1{\cdot}35$, all the curves become straight lines and more or less parallel to each other. For a given value of $Nu/(Nu)_0$, the Prandtl number effect can also be seen from the decrease of K with the corresponding increase of Pr. The above observation for Prandtl number effect on heat transfer result also confirms the role of Prandtl number in the convective terms of the energy equation (11) noted earlier. A study of the basic equations shows that when the Prandtl number

is large, the inertia terms in the momentum equations (8) and (10) can be neglected. This fact is also verified by the numerical results. In other words, while the secondary flow is rather weak, the convective terms in the energy equation (11) are important because of large Prandtl number. With large Prandtl number it can be shown that a new parameter K^2Pr results.

energy equation. Alternatively, by normalizing the dimensional momentum equation for secondary flow corresponding to equation (8) and the energy equation (5), the parameter K^2Pr can also be shown to arise.

It is now possible to obtain a new correlation of heat transfer results for high Prandtl number fluids as shown in Fig. 11 where all the results

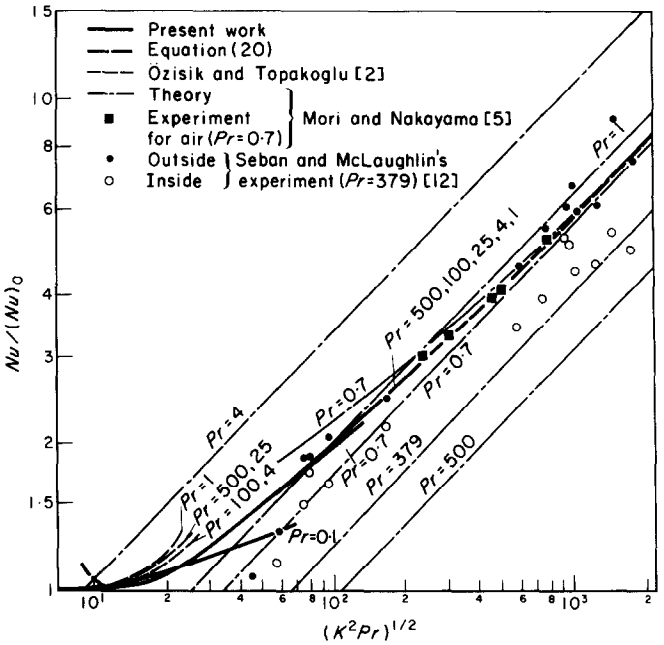

FIG. 11. Comparison of a new correlation curve for heat transfer results for $Pr \geqslant 1{\cdot}0$ from this work using a new parameter with theoretical and experimental results available in literature.

For example, by introducing the secondary flow characteristic velocity U_c, characteristic axial velocity $\overline{W}$ and other suitable characteristic quantities for $T - T_w$, P' and Ω, the radial momentum equation (2) and the energy equation (5) may be normalized. Noting that the centrifugal force term and the viscous terms in the momentum equation must be of the same order of magnitude, one obtains $U_c/\overline{W} = Re(a/2R_c)$. Using this relation, the new parameter K^2Pr can be shown to appear as a coefficient of the convective terms in the normalized

presented in Fig. 10 are replotted on the basis of $Nu/(Nu)_0$ vs. $(K^2Pr)^{\frac{1}{2}}$ for illustration. Since Seban and McLaughlin's experimental data [12] are for fluids with Prandtl number ranging from 100 to 657, the arithmetic mean value of 379 is taken as a value of Prandtl number for simplicity in replotting. It is significant to note that with the new correlation all the theoretical curves for $Pr \geqslant 1$ from the present analysis nearly coincide, and in particular the results for $Pr = 1$, 4, 25, 100 and 500 coincide exactly. This suggests the practical implication of "large"

Pr. Furthermore, all the experimental data for $Pr = 379$ and 0·7 (air) are seen to scatter within a narrow band around a new correlation curve with a higher Dean number portion obtained by a linear extrapolation of the present theoretical results. The agreement between a new correlation curve and the available experimental data is considered to be remarkable in view of the fact that the new correlation is based on the assumption that the Dean number is small and the Prandtl number is large. Furthermore, one should note the inherent difficulties in the experimental measurements and the experimental simulation of the thermal boundary condition such as the uniform peripheral wall temperature at any cross section. The following approximate equation is deduced using the new parameter K^2Pr as the curve to best fit all the numerical results.

$$Nu/(Nu)_0 = 0{\cdot}181\,Q(1 - 0{\cdot}839Q^{-1} + 35{\cdot}4\,Q^{-2} - 207\,Q^{-3} + 419\,Q^{-4}) \quad (20)$$

where, $Q = (K^2Pr)^{\frac{1}{2}} \geqslant 3{\cdot}5$ for $Pr \gtrsim 1$

For $Q \leqslant 3{\cdot}5$, the secondary flow effect is estimated to be less than 1·5 per cent in terms of the Nusselt number ratio $Nu/(Nu)_0$. In view of the possible experimental errors in the region $Q \leqslant 3{\cdot}5$, the secondary flow effect is not considered to be important in that region. The correlation equation (20) can now be considered to be valid for all the practically important laminar regimes with sufficient accuracy. In the application of the correlation equation (20) to the flow regime where the Dean number K is greater than say 200, it is well to note that secondary flow stabilizes laminar flow with the transition Reynolds numbers of 6000–8000 being characteristic of helically coiled tubes [14] and also the present analysis is valid up to $a/R_c = 0[10^{-1}]$.

The inconsistent behavior of the boundary layer approximation [5] for the Prandtl number effect is evident from Fig. 11. For example, the heat transfer results for $Pr = 1, 4$, and $Pr = 379$, 500, are clearly on the opposite sides of the new correlation curve. This leads to the conclusion that the boundary layer approximation [5] is valid only near $Pr = 1{\cdot}0$.

A comment on the computing time required to obtain a complete numerical result for flow and heat transfer at each value of the parameter C^2/r_c may be of interest. It takes about 2 min for $C^2/r_c = 10^3$ and 8 min for $C^2/r_c = 4 \times 10^4$ with $M, N = 28$ and $Pr = 1{\cdot}0$ on IBM 360/67. On the other hand, a computing time of approximately 40 min is required to obtain a complete result up to $C^2/r_c = 4 \times 10^4$ with $M, N = 28$ and $Pr = 1{\cdot}0$. One notes that the computing time depends to a large extent on the selection of a relaxation factor.

5. CONCLUDING REMARKS

1. The numerical solution using a combination of the line iterative method and boundary vorticity method is shown to be very effective up to a reasonably high value of the Dean number where an asymptotic behavior already appears for flow and heat transfer results, and further result for high Dean number range can be obtained by a linear extrapolation. The distinctive features of the new method are its simplicity, computational stability, and a significant saving in computing time as compared with the conventional methods.

2. The Prandtl number effect for fully developed laminar forced convection in curved pipe is clarified for the first time. It is shown that all the heat transfer data for the present problem can be correlated by a single curve using a new parameter $Q = (K^2Pr)^{\frac{1}{2}}$ for $Pr \geqslant 1$. This observation of the asymptotic behavior in heat transfer results for Prandtl number effect is noteworthy and significant. It is not required in future to carry out separate computation or experiment for various Prandtl numbers in order to study the Prandtl number effect for $Pr \geqslant 1$.

3. According to the order of magnitude analysis, the present formulation is considered

to be valid for $a/R_c \leqslant 0[10^{-2}]$. However, it is of practical interest to note that the assumption 1 in the formulation of the problem may be considered to be valid up to $a/R_c = \frac{1}{10}$ in practice. This observation is based on the theoretical and experimental flow results available in the literature [10, 11, 14]. Reference [14] appears after the submission of the present paper and is included here for completeness.

4. The correlation equation (20) clearly indicates the existence of the asymptotic behavior for large Prandtl number or large Dean number, and only the first term on the right hand side of equation (20) is significant. This finding is similar to that observed in earlier work [13] and is considered to be of practical importance.

5. Based on the present numerical results it is now evident that the perturbation method as used in the literature diverges quickly with the increase of the Dean number. This remark applies to a class of broadly similar forced laminar convection problems with secondary flow. Furthermore, it is shown that the boundary layer approximation predicts inconsistent Prandtl number effect and is valid only near $Pr = 1{\cdot}0$.

6. The question arises as to the physical signficance of the tube wall thermal boundary conditions employed in the numerical analysis. It is known that laminar flow heat transfer in ducts is strongly influenced by the wall boundary condition—uniform wall temperature around the duct, uniform wall temperature axially, uniform heat flux axially or around the duct. The particular boundary condition of constant heat input per unit axial length and constant peripheral wall temperature at a given axial position can be met in practice only with the wall of large thermal conductivity in the peripheral direction. Nevertheless, this is considered to be one of the basic thermal boundary conditions in the literature. The particular thermal boundary condition was selected to demonstrate the applicability of the boundary vorticity method to the present problem, and to compare the numerical results for heat transfer with the published theoretical and experimental data. It is to be noted that the method employed can be readily adapted to various other thermal boundary conditions mentioned earlier. Further details regarding the thermal boundary conditions in convective heat transfer can be found in [15].

ACKNOWLEDGEMENTS

This work was supported by the National Research Council of Canada through Grant NRC A1655. The authors wish to thank Dr. Guang-Jyh Hwang for helpful discussion regarding boundary vorticity method, and Mrs. E. S. Buchanan for typing the manuscript.

REFERENCES

1. W. R. Dean, Note on the motion of fluid in a curved pipe, *Phil. Mag.* **4**, 208–223 (1927).
2. M. N. Özisik and A. C. Topakoglu, Heat transfer for laminar flow in a curved pipe, *J. Heat Transfer* **90**, 313–318 (1968).
3. M. Adler, Strömung in gekrümmten rohren, *Z. Angew. Math. Mech.* **14**, 257–275 (1934).
4. S. N. Barua, On secondary flow in stationary curved pipes, *Q. J. Mech. Appl. Math.* **16**, 61–77 (1962).
5. Y. Mori and W. Nakayama, Study on forced convective heat transfer in curved pipes (1st report, Laminar region), *Int. J. Heat Mass Transfer* **8**, 67–82 (1965).
6. G. J. Hwang and K. C. Cheng, Boundary vorticity method for convective heat transfer with secondary flow—application to the combined free and forced laminar convection in horizontal tubes, *Heat Transfer* 1970, *Proc. Fourth International Heat Transfer Conference*. Vol. 4, NC 3.5. Elsevier, Amsterdam (1970).
7. G. J. Hwang, Thermal instability and finite amplitude convection with secondary flow, Ph.D. thesis, University of Alberta, Edmonton, Alberta, Canada (1970).
8. P. H. Newell, Jr. and A. E. Bergles, Analysis of combined free and forced convection for fully developed laminar flow in horizontal tubes, *J. Heat Transfer* **92**, 83–93 (1970).
9. M. R. Samuels and S. W. Churchill, Stability of a fluid in a rectangular region heated from below, *A.I.Ch.E.Jl* **13**, 77–85 (1967).
10. C. M. White, Streamline flow through curved pipes, *Proc. R. Soc.* **123A**, 645–663 (1929).
11. H. Ito, Laminar flow in curved pipes, *Z. Angew. Math. Mec.* **49**, 653–663 (1969).
12. R. A. Seban and E. F. McLaughlin, Heat transfer in tube coils with laminar and turbulent flow, *Int. J. Heat Mass Transfer* **6**, 387–395 (1963).
13. K. C. Cheng and M. Akiyama, Laminar forced convection heat transfer in curved rectangular channels, *Int. J. Heat Mass Transfer* **13**, 471–490 (1970).

14. L. C. TRUESDELL, JR. and R. J. ADLER, Numerical treatment of fully developed laminar flow in helically coiled tubes, *A.I.Ch.E.Jl* **16**, 1010–1015 (1970).

15. T. F. IRVINE, JR., Noncircular duct convective heat transfer, *Modern Developments in Heat Transfer*, edited by W. IBELE, pp. 1–17. Academic Press, New York and London (1963).

METHODE DE VORTICITE LIMITE POUR UN TRANSFERT THERMIQUE PAR CONVECTION FORCEE LAMINAIRE DANS DES TUYAUX COURBES

Résumé—Une solution aux différences finies utilisant une combinaison d'une méthode itérative linéaire et d'une méthode de vorticité limite est présentée pour la convection laminaire forcée complètement développée hydrodynamiquement et thermiquement dans des tuyaux courves soumis aux conditions thermiques limites de flux thermique pariétal uniforme et de température pariétale uniforme sur la péripherie pour une position axiale quelconque. La solution numérique converge jusqu'à un nombre de Dean raisonnablement grand où le comportement asymptotique des résultats relatifs à l'écoulement et au transfert thermique apparait déjà. L'effet du nombre de Prandtl sur le résultat du trasfert thermique est clarifié pour la première fois, et on-montre que tous les résultats du transfert thermique pour $Pr \geqslant 1$ peuvent être reliés par une simple courbe utilisant un nouveau paramètre ($K^2\ Pr$) avec une précision raisonnable. On compare les résultats numériques de la présente analyse avec les résultats expérimentaux et théoriques utilisables dans la littérature. On montre facilement que la méthode de perturbation est inadéquate et on relève une certaine déficience de la méthode d'approximation de la couche limite.

RANDWIRBELMETHODE FÜR LAMINARE ZWANGSKONVEKTION. WÄRMEÜBERTRAGUNG IN GEKRÜMMTEN ROHREN

Zusammenfassung—Unter Benützung einer Kombination aus der Methode der Linieniteration und der Randwirbel wird eine Lösung mit endlichen Differenzen gegeben für hydrodynamisch und thermisch vollentwickelte laminare Zwangskonvektion in gekrümmten Rohren, die abhängt von den Randbedingungen eines über die Rohrlänge konstanten Wärmestromes durch die Rohrwand und einer konstanten Wandtemperatur am Umfang eines beliebigen Axialschnittes. Die numerische Lösung konvergiert bis zu einer vernünftigen Dean-Zahl, wo bereits das asymptotische Verhalten für die Ergebnisse aus Strömung und Wärmeübertragung auftritt. Die Wirkung der Prandtl-Zahl auf den Wärmeübergang wird zum ersten Mal geklärt. Es zeigt sich, dass alle Ergebnisse des Wärmeübergangs für $Pr \geqslant 1.0$ durch eine einzige Kurve aufeinander bezogen werden können. Der neue Parameter ($K^2 \cdot Pr$) liefert dies mit guter Genauigkeit. Die Rechenergebnisse aus dieser Analyse werden mit den experimentellen und theoretischen Ergebnissen aus der Literatur verglichen. Die Verwirbelungsmethode erweist sich klar als unzureichend. Auch die Näherungsmethode der Grenzschicht zeigt gewisse Nachteile.

МЕТОД ГРАНИЧНЫХ ВОЗМУЩЕНИЙ ДЛЯ РАСЧЁТА ТЕПЛООБМЕНА В ИСКРИВЛЕННЫХ ТРУБАХ ПРИ ЛАМИНАРНОЙ ВЫНУЖДЕННОЙ КОНВЕКЦИИ

Аннотация—Представлено решение в конечных разностях, полученное с помощью совместного применения метода линейных итераций и метода граничных возмущений, для вынужденной конвекции, полностью развитой гидродинамически и термодинамически, в искривленных трубах при тепловых пограничных условиях для одинакового по оси теплового потока стенки и одинаковой по периферии температуры стенки в любом месте по оси. Численное решение сходится для достаточно высоких чисел Дина, где уже проявляется асимптотический характер результатов для течения и теплообмена. Впервые выясняется влияние числа Прандтля на данные по теплообмену; показано, что все результаты по теплообмену для чисел $Pr \geqslant 1{,}0$ можно с достаточной точностью обобщить одной кривой, используя новый параметр (K^2Pr). Численные результаты данного анализа сравниваются с экспериментальными и теоретическими данными, имеющимися в литературе. Убедительно показано, что метод возмущений является несостоятельным и указываются определённые недостатки метода аппроксимаций пограничного слоя.